

Physical Characterization and Rheological Behavior of AA 2017 Powder Modified with Al-5.0Nb-0.5B Inoculant Powder for Laser-based Powder Bed Fusion

Pamela Karina dos Santos Bomfim^{a,*} , Bruna Fernanda Batistão^a, Flavia Costa da Silva^{b,c} ,
Vitor Eduardo Pinotti^a, Moyses Leite de Lima^c , Francisco Gil Coury^{a,d} , Piter Gargarella^{a,d,e} 

^a Universidade Federal de São Carlos, Programa de Pós-Graduação em Ciência e Engenharia de Materiais, Rod. Washington Luiz, Km 235 SP-310, 13565-905, São Carlos, SP, Brasil.

^b Universidade de São Paulo, Escola de Engenharia, Departamento de Engenharia de Produção, Av. Trabalhador São Carlense, 400, 13566-590 São Carlos, SP, Brasil.

^c Instituto de Pesquisas Tecnológicas, Laboratório de Processos Metalúrgicos, Av. Prof. Almeida Prado, 532, 05508-901, São Paulo, SP, Brasil.

^d Universidade Federal de São Carlos, Departamento de Engenharia de Materiais, Rod. Washington Luiz, Km 235 SP-310, 13565-905, São Carlos, SP, Brasil.

^e Universidade Federal de São Carlos, Centro de Caracterização e Desenvolvimento de Materiais, Rod. Washington Luiz, km 235 SP-310, 13565-905, São Carlos, SP, Brasil.

Received: September 29, 2023; Revised: December 27, 2023; Accepted: February 20, 2024

Blending finer powders of Ti, Zr, Ta, Sc, and Nb compounds as inoculants have been a promising strategy to modify precipitation-hardened aluminum alloys for laser-based powder bed fusion, promoting a crack-free equiaxed microstructure. However, there is still a lack of comprehensive understanding of the influence of these fine Al-Nb-B inoculant particles on the AA 2017 powder's physical characteristics and flowability during the process. The results indicate that blended powder has a similar PSD to AA 2017 powder. Furthermore, the circularity, smoothness, and morphology of the particles indicate that both inoculant and AA2017 powders do not exhibit high sphericity, but the blended powder showed slightly more agglomerated particles. Regarding rheological properties, it was observed that a higher flow energy was required to move the blended powder in unconfined conditions compared to the AA 2017 powder. Additionally, the blended powder exhibited higher compressibility and tendency to retain air in packed conditions during the deposition and spreading process. In conclusion, the physical characterization techniques combined with rheological tests have proven to be a rapid and reliable approach for assessing the impact of the finer inoculant particles' characteristics on the laser-based powder bed fusion.

Keywords: Aluminum alloys, inoculation, powder flowability, laser - based powder bed fusion.

1. Introduction

Laser-based Powder Bed Fusion (L-PBF), also known as Selective Laser Melting (SLM), stands out for allowing the production of customized and complex parts, often considered a cost-saving and energy-saving processing route for some parts in the aerospace, automotive, and military defense industries¹. However, a limited number of alloys are "easily printed" during the L-PBF process^{1,2}. In the context of aluminum alloys, despite the increasing demand for lightweight structures, only the Al-Si-Mg alloys system is considered printable^{2,3}, whereas most precipitation-hardened alloys such as those from series 2XXX, 6XXX, and 7XXX display problems during L-PBF processing¹⁻³. These later alloys typically have large solidification ranges making them more susceptible to hot tearing at columnar grain boundaries^{2,3}. The hot tearing occurs during the last stage of solidification because the liquid film remaining within the dendritic/columnar grains cannot support the strain generated

by the solidification shrinkage and thermal contraction^{4,5}. At this stage, the mushy zone presents a low permeability and high viscosity, making it difficult to fill any openings at the grain boundaries^{4,6}. The use of alloying elements such as Ti, Zr, Sc, Ta, and Nb is proposed to mitigate this problem due to the in-situ formation of heterogeneous nucleation particles such as TiAl₃, Al₃Zr, Al₃Sc, Al₃Ta, and Al₃Nb, respectively^{1,2,7,8}. These Al₃X particles in the melt pool can change the solidification from columnar to equiaxed and diminish crack formation^{2,7,8}.

A successful example of these additions was given by Agrawal et al.⁸. They obtained crack-free AA 2024 L-PBF samples when approximately 3.78 wt% Zr in the form of micrometric particles was mixed with the alloy powder. The mixture resulted in a fully equiaxed microstructure of high strength. Similarly, the addition of 0.8 wt% Sc to an AA 2024 alloy also led to crack-free samples during the L-PBF process⁸. Tan et al.¹ also produced crack-free AA 2024 L-PBF samples with an equiaxed and refined microstructure after

*e-mail: pamelasbomfim@ppgcm.ufscar.br

adding 1.0 wt% Ti nanoparticles. Approximately 5.4wt% of Tantalum nanofunctionalized particles were also tested as inoculants in an AA 7075 alloy. The result was also crack-free samples with a high grain refinement⁹. Xiao¹⁰ and Wang et al.² inoculated AA 7050 alloy with 1.5 and 3.0 wt% Nb nanoparticles, respectively, using powders mixing and reported a complete transformation of columnar to equiaxed grains due to the excellent nucleation ability of Al₃Nb.

However, prior to producing L-PBF parts using modified aluminum alloys, the powder characterization should be performed because powders have a key role in the efficiency of the L-PBF process. In other words, spherical morphology tends to flow better, and wider particle size distribution will ensure that finer particles are available to fit into the voids of the larger particles, which leads to parts with higher density and strength and better surface finish^{11,12}.

Previous works have highlighted that conventional powder characterization assessments, such as particle morphology, particle size distribution, apparent density, and flowability behavior using a standardized funnel, are often unsuitable, especially for aluminum powders that usually show complex cohesive behavior, which dictate the flow behavior^{13,14}.

On the other hand, although Strondl et al.¹⁵ reported that some conventional characterization techniques coupled with powder's rheology and dynamic analysis might successfully predict the flow behavior during L-PBF, only a few works have investigated the properties of metallic powders using these methods¹⁵.

In the L-PBF process, spherical and smooth-surfaced particles are preferable, which allow a more uniform powder flow during powder bed formation. In contrast, particles with irregularities on the surface tend to suffer from mechanical interlocking, which impairs flowability and, consequently, reduces the powder bed packing density¹⁵⁻¹⁷. Particle morphology is often analyzed by Scanning Electron microscopy (SEM) and/or Dynamic Image Analysis (DIA). This method provides detailed and high-resolution surface characterization and allows the estimation of numerous shape parameters such as smoothness and circularity, both values indicating the (non-)spherical shape of the particles. Values closer to 1 suggest the presence of particles with a rounder shape. Araújo et al.¹¹ found that Al-Fe-Cr-Ti alloys powders manufactured by gas atomization using different atomizers presented circularity above 0.92, which increases as the particles become smaller.

Regarding particle size distribution, most powders for L-PBF consist of fine powders typically in the range of 20-63 μm as the layer thickness is dictated by the particle size¹⁸. According to Vock et al.¹⁴, PSD is widely evaluated due to its ability to influence layer densities in L-PBF. For instance, broader PSDs are desirable to achieve higher layer densities, while a narrower PSD distribution is preferable for powder flowability, with coarser particles that have lower attractive forces resulting in better flowability^{14,16,19,20}.

Several techniques have been used for particle size measurement, i.e., sieving, dynamic image analysis, laser diffraction, air permeability, and X-ray diffraction. These techniques, such as Sieving and Laser Scattering, operate assuming the particles are spherical and may be inadequate for fine powders (particle size less than 50μm), but for

dynamic image analysis^{21,22}. Laser Scattering coupled with particle evaluation using Dynamic Image Analysis allow us to determine particle distribution, also obtaining parameters that describe the particle in terms of average diameter, superficial area, and mean perimeter. Furthermore, this technique is attractive for its relatively low cost, less time-consuming, ability to provide morphological information and high effectiveness for fine particles²¹.

ASTM F3049²³ defines tests to measure powder flowability for the L-PBF process. Some methods described in this standard, such as Hall or Carney's funnel and Hausner ratio, are considered by some works^{15,24} to be inefficient in distinguishing powders for L-PBF, as they originated from the traditional powder metallurgy techniques. Therefore, the FT4 rheometer, also known as a flow tester, has become increasingly popular, especially in pharmaceutical industries, not in the L-BF process, despite allowing the correlation of rheology properties with powder bed formation²⁵.

It is well known that gas atomized aluminum particles tend to have imperfections, such as satellites and irregularly shaped particle agglomerates, making the powder flow even more difficult due to mechanical interlocking forces^{25,26}. It has also been observed that although powder blending has shown a promising route to modifying aluminum alloys for the L-PBF process, it involves particle-particle and particle-wall collisions, which leads to strong cohesion among particles and accumulation of electrostatic charges²⁵. In addition, a long blending time may also lead particles to be smashed into a flat or highly distorted shape^{2,10}. Therefore, due to the high cohesiveness of the particles, the FT4 rheometer would be a more appropriate measurement method for these cases.

Given the context, the most relevant studies showed promising results using the inoculation process through the mixture of atomized finer powders (smaller size < 20 microns) or even nanoparticles^{1,2,9,10}.

While nano-scale inoculants have gained widespread adoption in the L-PBF process, resulting in significant thermal undercooling, their use poses a higher safety risk than micrometric particles. In addition, they tend to agglomerate, impeding the achievement of homogeneous mixing, as noted by Tan et al¹. Studies have been performed on micron-scale inoculants, but they are few and mainly focus on TiB₂. For instance, Wang et al.²⁷ mixed 5 vol% TiB₂ with AA 2024 alloy and achieved significant grain refinement, reducing the grain size from approximately 23μm to 2.5μm.

Conversely, Elambasseril et al.²⁸ recently reported on fabricating AA 2019 alloy with Al-5.0Ti-1.0B using L-PBF, demonstrating a significantly reduced crack fraction and aluminum grain size. However, they did not observe a columnar-equiaxed transition (CET).

Based on these recent findings regarding the Al-Ti-B inoculant in the L-PBF process, and considering the abundance of niobium in Brazil, we have chosen to utilize the novel Al-5.0Nb-0.5B inoculant produced by the Brazilian Metallurgy and Mining Company (CBMM®). Therefore, our objective is to evaluate the properties of AA2017 alloy powders, both with and without the addition of microparticles from Al-5.0Nb-0.5B inoculant, and to explore the relationships of these properties with the samples produced through the L-PBF process.

2. Materials and Methods

AA 2017 ingots were prepared from elements with purity above 99.5% using an induction furnace Inductotherm 50-30R, while Al-5.0Nb-0.5B ingots were supplied by CBMM Ltd (Brazil). Both the AA 2017 and Al-5.0Nb-0.5B ingots were gas atomized separately in a PSI – HERMIGA under a gas atomization pressure of 40 bar and 46 bar, nozzle diameter of 2.0 mm and 2.5 mm, a gas-metal ratio of 3.7 m³/kg and 2.9 m³/kg, and an atomization temperature of 710 °C and 1492 °C, respectively, which is around 70 °C above the alloys liquidus temperatures. These parameters were established to obtain spherical powders as well as the PSD suitable for the L-PBF process. When the atomization process was completed, the powders were cooled down to room temperature in an argon atmosphere. In order to characterize the resulting powders, they were sieved, and the AA 2017 powder was blended with 2 wt% Al-5.0Nb-0.5B inoculant powder using a Turbula T2F shaker-mixer for 120 minutes at a speed of 70 rounds per minute. The chemical compositions of the feedstock powders were determined by inductively coupled plasma optical emission spectroscopy (ICP-OES) and are shown in Table 1.

2.1. Particle size distribution, circularity, and smoothness

The particle size distribution was measured using Laser Diffraction Particle analyser (HORIBA 930). The dispersion of approximately 2g of each powder sample was carried out in a liquid medium using ethyl alcohol (95%).

In addition to particle size distribution, circularity and smoothness were also calculated from particle images captured and processed by Dynamic Image Analysis. Circularity (C) Equation 1 is defined as the degree to which the particle is similar to a circle taking into account the bounding circle diameter (D_{BC}), while smoothness (S) Equation 2 is correlated to the area of the circle (A) and the perimeter of the particle's projection (P). Irregularities on the perimeter are indications of surface roughness. The maximum value calculated for the mentioned parameters is 1 for a perfect and smooth sphere²⁹.

$$\text{Circularity} = \frac{4A}{\pi D_{BC}^2} \quad (1)$$

$$\text{Smoothness} = \frac{4\pi A}{P^2} \quad (2)$$

2.2. Skeletal density

An AccuPyc 1330 gas pycnometer was used to measure the true density of the powders according to ASTM B 923³⁰.

The powders were weighed and poured inside a calibrated cylinder (6.5974 cm³), and helium gas was used as the displacement medium. The difference in pressure before and after the gas expansion was measured to calculate the volume and, consequently, the true density of the powders. Each powder sample was measured by five independent tests to ensure the accuracy of the measurement.

2.3. Morphology and microstructure

To obtain more information about powders' shape and morphology, the FEI Scanning Electron Microscopy (SEM) equipment was used, operating at 25 kV and equipped with energy-dispersive X-ray spectroscopy (EDX) system. Furthermore, the cross-sections of the powders were prepared using a standard metallographic procedure of grinding and polishing with chromium oxide paste and 1 μm diamond paste to investigate the microstructure of the powders.

2.4. Rheological properties of powder

For powder rheological evaluation, an FT4 rheometer (Freeman Technology Ltd., Tewkesbury, U.K.) was used on the AA2017 powder and the powder mixture AA 2017+2% Al-5.0Nb-0.5B. First, the powders were pre-treated for drying in an oven at 100°C for 12 h to remove the influence of moisture on flowability. Next, the powders were evaluated to determine the flow performance under different conditions. For this, seven testing setups were selected: dynamic, aeration, permeability, tapped, consolidation, compressibility, and shear testing modes. For each testing setup presented, the measurements were replicated three times for each powder, and the average and standard deviation values were calculated. The setup for each condition will be presented next.

2.4.1. Powder characterization under dynamic flow condition

The conditioning and dynamic tests were performed using a glass vessel with a plain base and a blade. A splitting device, specific to the equipment, was used to provide a fixed powder volume and mass of powder. The first step consisted of gently disturbing the powder using the blades as it enters the powder and turning it clockwise to reduce the stress between particles, remove excess air, minimize the effect of powder handling, homogenize the sample, and create a powder bed for subsequent flow measurements³¹. This procedure step is called conditioning.

After the conditioning cycle, the precise volume of the powder can be seen through by split vessel device. While the powder remaining in the lower container after splitting was weighed by the FT4 rheometer scale, and the conditioned bulk density (CDB) in g/cm³ was calculated according to Equation 3. Therefore, CBD can be used with the tapped density (obtained under packed condition)³¹.

Table 1. Chemical composition of the powders (wt%).

Powders	Cu	Mg	Mn	Fe	Si	Nb	B	Al
AA 2017	4.4 ± 0.4	0.6 ± 0.0	0.7 ± 0.0	0.5 ± 0.1	0.4 ± 0.0	-	-	bal
Al-5.0Nb-0.5B	-	-	-	0.1 ± 0.0	0.2 ± 0.0	5.3 ± 0.4	0.46 ± 0.0	bal
AA 2017+2%Al-Nb-B	4.8 ± 0.2	0.6 ± 0.0	0.7 ± 0.0	0.6 ± 0.0	0.4 ± 0.0	0.04 ± 0.0	-	bal

$$\text{Conditioned Bulk Density (CBD)} = \frac{\text{Split Mass}}{\text{Split Volume}} \quad (3)$$

Afterward, eight measurements were performed where a descent followed by an ascent rotating blade movement with a predetermined helical path and constant blade tip speed of 100 mm/s was used to determine the powder-specific energy (SE) and the stability index (SI). In fact, Specific Energy and Stability Index were measured during the first descent (FE_{D1}), the sixth ascent (FE_{A6}), the seventh descent (FE_{D7}), and the seventh ascent (FE_{A7}), and calculated using Equation 4 and Equation 5, respectively³².

$$\text{Specific Energy (SE)} = \frac{(FE_{A6} + FE_{A7})}{2} / \text{Split mass} \quad (4)$$

$$\text{Stability Index (SI)} = \frac{FE_{D7}}{FE_{D1}} \quad (5)$$

SE measures the energy required to promote the flow of unconfined powder, which mainly relates to cohesion between particles and other physical properties, such as particle size, shape, and texture. In contrast, SI checks the stability of the powder during the tests, and values closer to 1 indicate higher stability. This means that the powder did not suffer alteration during the test, explaining the relationship between the last and first measures³². In addition, two metrics were also recorded, the Basic Flow energy (BFE) and the Flow Rate index (FRI). BFE represents the flow energy measured during the seventh descent path (FE_{D7})³³, which depends on many powders' parameters such as size distribution, shape, density, cohesion, humidity, electrostatic forces, state of compaction (air content), etc. Flow Rate index (FRI) corresponds to the flow energy ratio between the eighth and eleventh descents (FE_{D8} and FE_{D11} , respectively) from Equation 6. This measures the behavior of the powder to the variation of the flow rate caused by the variation in the blade descent speed.

$$\text{Flow Rate Index (FRI)} = \frac{FE_{D11}}{FE_{D8}} \quad (6)$$

The last test in dynamic flow mode was the tapped density by a total of 50 taps in a dispositive³⁴, and the Consolidated Energy (CE) was measured, which can be compared to the BFE.

2.4.2. Powder characterization under aerated conditions

The sensitivity of the flowability due to nitrogen flow was evaluated using an aeration test. A Ø25 x 35 mm vessel was used with a stainless-steel porous base through which nitrogen is introduced to the base of the powder bed. The aeration program follows three sequential steps n (conditioning/descent/ascent of the rotation blade at 100 mm/s), which were repeated five times on each powder sample subjected to superficial nitrogen velocities varying from 1 to 4 mm/s. The Aeration Energy value was recorded during the descent movement, with airflow at 4 mm/s (AE_4), as described in Equation 7.

The Aeration Rate, which means aerating capabilities, was determined by the ratio of the blade movement without airflow (AE_0) with movement at airflow at 4 mm/s (equivalent to a volumetric flow rate of around 2000 mm³/s), calculated by Equation 8³⁵.

$$\text{Aeration Energy (AE)} = \text{Energy (air velocity } n_4) \quad (7)$$

$$\text{Aeration Rate (AR)} = \frac{AE_0 (\text{air velocity } n_0)}{AE_4 (\text{air velocity } n_4)} \quad (8)$$

The extent to which Aeration Energy is reduced depends on many powders' physical properties, such as cohesion, particle shape, texture, and density. This test is important within the L-PBF process as it evaluates the tendency of powders to agglomerate, being that high AE ($AE > 20$) is ideal to obtain a uniform powder layer. In contrast, AE equal 1, the powders are not sensitive to aeration, therefore, are usually very cohesive.

2.4.3. Powder characterization under packed condition

The Permeability test measures the ease with which the powder bed releases the entrapped air³⁶. The nitrogen at constant velocity (2 mm/s) was introduced at the bottom of the powder column into the glass vessel, and increasing levels of compressive force were applied with a porous piston (from 1 kPa to 15 kPa). During the test, the air pressure was monitored as a function of the applied load, and the permeability was calculated.

In addition to the permeability test, the compressibility test was also carried out to measure the degree of cohesiveness of the particles. In this test, the density's change is measured as a function of applied stress, and, in other words, as the strength is used, air exits among the particles, which leads to the accommodation of the powder in a smaller volume inside of the glass vessel³⁷.

From the Compressibility test, the compressibility metric (CPS) was calculated using conditioned volume (V_{cond}) and compressed volume (V_{comp}) as shown in Equation 9³⁷.

$$\text{Compressibility (CPS)} = \frac{V_{\text{conditioned}} - V_{\text{compressed}}}{V_{\text{compressed}}} * 100 \quad (9)$$

Both tests are influenced by many physical properties of the powder, such as particle size and distribution, cohesiveness, shape, surface texture, and bulk density.

The factor by which the flow energy has increased in relation to the value of BFE is given by the Consolidation Index (CI), the ratio between CE and BFE as indicated in Equation 10.

$$\text{Consolidation Index (CI)} = \frac{\text{Consolidated flow energy (CE}_{\text{tapped}})}{\text{Basic flow energy (BFE)}} \quad (10)$$

2.4.4. Powder characterization under shear condition

The Shear measurement quantifies the ease with which the consolidated powder transitions from a static to a dynamic state, i.e., mimicking when powders start discharging from a hopper. Therefore, the shear stress test is initiated with

a previous compression cycle where 9 kPa is applied for 60 seconds using a vented piston while the shear stress becomes constant. At that point, the powder column reaches a steady-state flow, which defines the pre-shear point as reported as step *1 in Figure 1. Once the compression cycle is completed, the vented piston is replaced with the shear head. The shear head moves to the surface of the powder at a speed of 0.5 mm/s and then slowly moves down at a maximum speed of 0.08 mm/s until the target consolidating stress is re-established and held for 60 s, thus characterizing the pre-shearing cycle also known as the first step (Step *1).

During the shear cycle, the rotation of the shear head is initiated and gradually increased until the powder is flowing to obtain the shear yield stress. These steps, including pre-shearing, were repeated four times in order to draw a total of five yield points, which defines the second step (Step *2) in Figure 1.

The Cohesion parameter (τ_0), characterized as (Step*3), was obtained by fitting the previous five points and extending up to the ordinate axis. Indeed, it is obtained the shear stress where the trendline of the Yield locus intersects the y-axis.

Both Consolidation Stress (σ_1) and the Unconfined Yield Strength (σ_c) were obtained through one small and one large Mohr's circles tangent to the yield locus and passing the origin and pre-shear point, illustrating Step *4 and Step *5, respectively, in Figure 1^{38,39}.

The ratio between the normal stress applied to the powder lot (σ_1) and the unconfined yield strength (σ_c) resulted in the flow function parameter (ff_c), which is also used as a parameter for describing the flowability of powders according to the rheometer manufacturer.

2.5. Laser powder bed fusion process

Cubic specimens (5 x 5 x 5 mm) were fabricated by L-PBF under a protective argon atmosphere (Ar purity 99.999%) using OmniSint-160 equipment (OmniTek®) equipped with a 400 W Yb:YAG laser. The oxygen content in the L-PBF chamber was kept below 0.06% during the entire fabrication process.

The parameter optimization based on previous processing window tests was carried out using the following parameters: laser power varied between 250-300 W, the laser scanning speed between 400-2000 mm/s, the hatching spacing of 0.10 mm, and the layer thickness of 0.03 mm. For determining

heat input, the volumetric energy density (EV) Equation 11 was calculated by Wang et al.⁴⁰:

$$E_V = \frac{P}{V * H * T} \quad (11)$$

where P is the laser power input (W), V is the laser scanning speed (mm/s), H is the hatching spacing (mm) and T is the layer thickness (mm).

The density of all specimens (cast and 3D printing parts) were evaluated by the Archimedes method using a Gehaka density measuring set DSL 910 following the ASTM B962-13⁴¹ standard for this procedure. The average density value for the AA2017 cast samples was $2.713 \pm 0.004 \text{ g/cm}^3$, which was used to calculate Relative density.

3. Results and Discussion

3.1. Particle size distribution

The PSD curves of AA 2017, inoculant powder (Al-5.0Nb-0.5B) and blended powders (AA 2017 + 2% Al-5.0Nb-0.5B) are shown in Figure 2a, Figure 2b and Figure 2c, respectively. Comparing the curves, AA 2017 powder's curve is practically the same as blended powder, in contrast to the inoculant powder, which has a lower d_{50} , indicating this powder has a larger number of fine particles than the other powders.

Baitimerov et al.⁴² pointed out the importance of estimating the span of the distribution, which correlates the ratio $d_{90}-d_{10}$ with d_{50} through the PSD curves due to its influence on the flowability behavior. According to them, the lowest span has better flowability of the powder. The span of distribution for AA2017 was 1.0 and reduced to 0.9 when adding the inoculant which has a span of 1.2. In this case, the span was reduced because there was a reduction in d_{90} when adding the inoculant to the alloy, thus increasing the number of fine particles. Therefore, the blended powder is expected to show worse flowability due to the finer inoculant particles added.

In general, the blended powder has adequate PSD (15-50 μm) for L-PBF, in agreement with the literature (20-63 μm), more than AA 2017 powder (14-68 μm)¹⁸. On the other hand, it is known that powder that contains too small particles tends to fly up along the turbulence of inert gas flow during the process. At the same time, the laser needs more power to completely melt larger particles, resulting in printed parts with spattering, balling, and high surface roughness^{18,43}.

3.2. Morphology of particles and microstructure

The value of circularity and smoothness are summarized in Table 2. When these values are closer to 1, the particle tends to be more spherical and with a smoother surface^{11,16}. Therefore, it can be seen that AA 2017, Al-5.0Nb-0.5B and blended powders do not exhibit high sphericity. Moreover, the circularity and smoothness are not very close to 1, indicating irregularities in the powders' particles, as demonstrated by secondary electron images (Figure 3). It is possible to note the presence of satellites, some particles are not fully

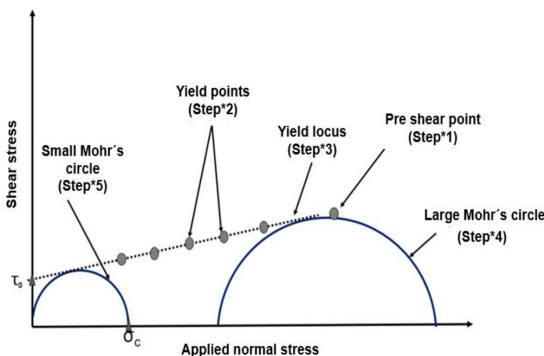


Figure 1. Schematic illustration of shear test methodology to obtain cohesion, unconfined flow stress and flow factor (adapted from ASTM D7891-15³⁸).

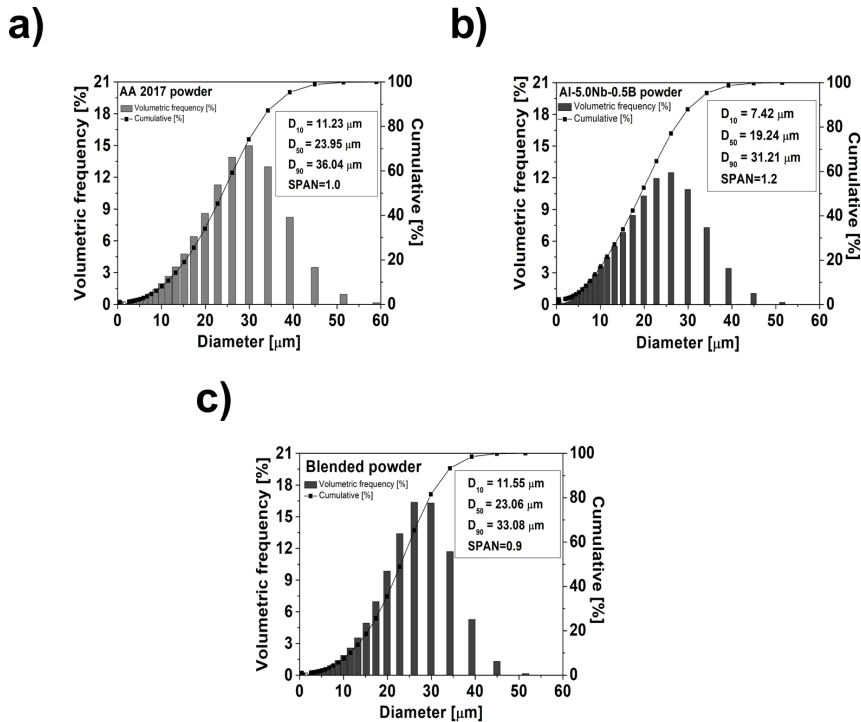


Figure 2. Volume and accumulated distribution as function of particle diameter for (a) AA2017 powder, (b) inoculant powder (Al-5.0Nb-0.5B) and (c) blended powder (AA 2017+2% Al-Nb-B).

Table 2. Circularity, smoothness and skeletal density of AA 201, Al-Nb-B inoculant and blended powders.

Powders	Circularity	Smoothness	Density(g/cm^3)
AA 2017	0.713 ± 0.111	0.550 ± 0.128	2.834 ± 0.010
Al-5.0Nb-0.5B	0.671 ± 0.131	0.456 ± 0.152	2.772 ± 0.007
AA2017+2%Al-Nb-B	0.714 ± 0.110	0.560 ± 0.133	2.788 ± 0.003

spherical, and there are agglomerated particles, especially in the inoculant powder.

The skeletal densities of the atomized AA 2017, inoculant and blended powders are also shown in Table 2. The density of the AA2017 powder is higher than that of the inoculant and the blended powder, while the circularity degree is similar between AA 2017 and blended powder.

Figure 3 shows SEM images of the AA 2017, inoculant (Al-5.0Nb-0.5B) and the blended powder (AA 2017+ 2% Al-5.0Nb-0.5B), respectively. In Figures 3a and 3b, satellite particles can be seen attached to the larger spherical particles of the AA2017 powder. According to the literature⁴⁴, the formation of satellite particles occurs during droplet flight in the atomization process. Hence, a significant number of smaller particles collide with the larger particles due to their difference in velocity. In other words, small particles exhibit higher velocities at the nearest position below the nozzle than larger ones. As a result, smaller particles will weld on the larger particles' surfaces and be fully solidified⁴⁴.

The inoculant powder exhibits near-spherical morphology and a markedly significant fraction of fine and small particles, as shown in Figures 3c and 3d. Their particles are mostly

agglomerated, with minimal satellite content, while the blended powder (Figures 3e and 3f) depicts more irregular and agglomerated particles than AA 2017 powder. A priori, this could be attributed to the long mixing time applied (~2 hours) that would favor the particles' agglomeration. However, the literature predicts the mixing time to be around 2-4 hours^{10,44-46}. In this case, it seems that the particles' agglomeration is due to the inoculant's powder. This means that the atomization process parameters and intrinsic characteristics of the inoculant alloy promoted the agglomeration of the particles.

In general, the presence of satellites, agglomerated powder, and rougher particles negatively impair the powders' flow behavior and, consequently, powder bed densification. However, this adverse effect can be minimized using optimized processing parameters⁴⁰.

As shown in Figures 4a and 4c, fine cellular microstructures around 8.0 μm can be observed on the cross-sections of AA 2017 and blended powders. The microstructures are characterized by α -Al matrix surrounded by Cu-rich contour, besides no evidence of niobium-richer phases after the blended process in Figure 4c.

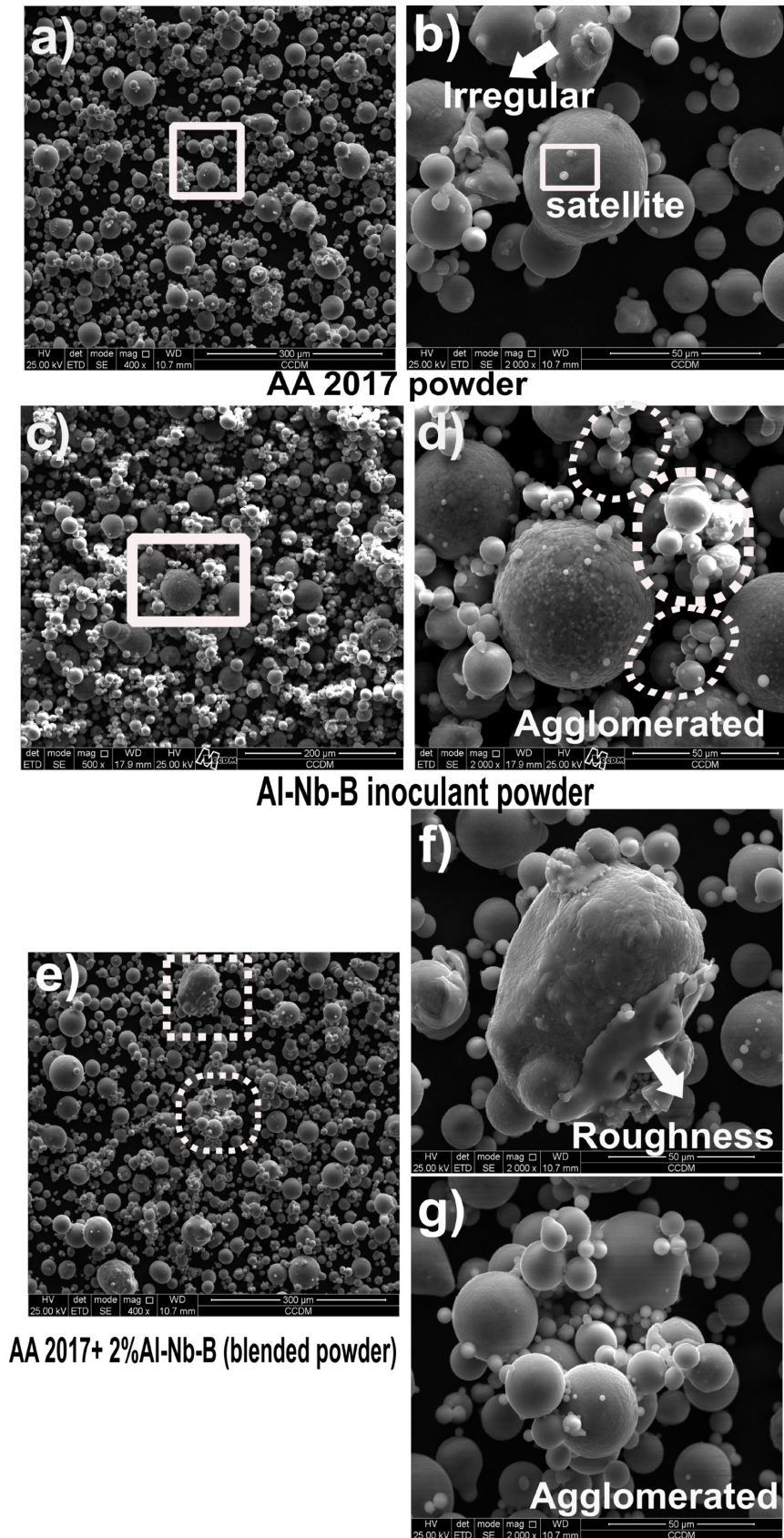


Figure 3. Secondary electron images (SEM) of: (a), (b) AA 2017 powder, (c), (d) Al-Nb-b inoculant powder and (e), (f) and (g) blended powder (AA 2017+ 2%Al-Nb-B).

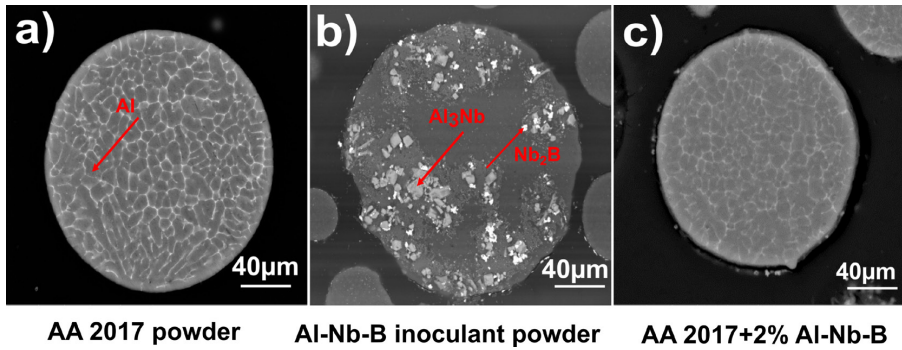


Figure 4. Cross-sections of powders: (a) AA 2017 powder; (b) Al-Nb-B inoculant powder; and (c) blended powder (AA 2017+2%Al-Nb-B).

For the inoculant powder (Figure 4b), it was possible to identify Al_3Nb and NbB_2 dispersed in the α -Al matrix as found by Li et al.⁴⁵, indicating that these phases could act as nucleation sites.

3.3. Rheological properties

3.3.1. Powder characterization under dynamic flow condition

Figure 5a presents the graph from the results of the CBD, together with the bulk tap density (BD_{tap50}). The blended powder has almost the same CBD value as the AA 2017 powder. Indeed, low CBD values indicate that the powders contain a high volume fraction of air³⁹. In contrast, the blended powder reached a slightly higher BD_{tap50} value than the AA 2017 powder, but both are consistent with the literature, which indicates around 1.60 g/cm^3 ³⁴⁶.

The higher BD_{tap50} value of the blended powder may be attributed to its high cohesiveness, which implies a greater amount of air trapped among particles. Thus, this air tends to escape after tapping, allowing particle packing. Moreover, as seen in Figure 5a, its particle size distribution is narrower, which means that fine inoculant particles may have fitted in voids of the AA 2017 powder larger particles¹¹.

The following parameters, including the SE, BFE, SI, and FRI were obtained from dynamic test results, and are also illustrated in Figures 5b, 5c, 5d and 5e.

SE measures the energy required to move the powder in the unconfined condition. It correlates well with the flow performance in low-stress conditions, particularly in L-PBF machines that involve the gravity powders' feedings where the powder is confined in contrast to the feeding powder by the vertical movement of a platform.

As a reference, the powder rheometer manufacturer mentions that most atomized powders exhibit $\text{SE} > 5$ ³². In the present study, the obtained values are lower, but comparing them, it is remarkable that much higher energy is required to move the blended powder ($\text{SE} = 3.26 \pm 0.12 \text{ mJ/kg}$) compared to the AA 2017 powder ($\text{SE} = 2.58 \pm 0.16 \text{ mJ/kg}$) (Figure 5b). This means there is greater cohesion and mechanical interlocking among particles in the blended powder due to the addition of finer particles^{15,47,48}, in addition to, as already mentioned, the presence of apparently more agglomerated particles in this powder (Figure 3f).

BFE is an important flowability factor, mainly to evaluate the influence of the addition of Al-5.0Nb-0.5B inoculant on the flow properties³³. As expected, the addition of smaller and agglomerated particles of inoculant affected the powder's flow⁴⁸, increasing its resistance to the forced flow by the blade. This difference in BFE values (Figure 5c) can be attributed to the presence of agglomerated and satellite particles (Figure 3b). Besides, finer particles in the blended powder may also contribute to cohesion among particles, as the interparticle forces are relatively more significant in smaller particles¹².

As recently estimated by Nguyen et al.⁴⁹, lighter powders need less energy to flow ($\sim 150 \text{ mJ}$) than heaviest powders, such as IN 718 powder alloy ($\sim 1032 \text{ mJ}$).

It is noteworthy that dynamic image analysis did not detect the difference in the number of irregular and agglomerated particles between powders, thus evidencing the need to combine techniques to obtain a more reliable characterization.

Powders exhibit both SI and FRI values (Figures 5d and 5e) within limits reported by the rheometer manufacturer. SI and FRI values are expected to be situated for most powders between $0.9 < \text{SI} < 1.1$ and $1.5 < \text{FRI} < 3.0$, respectively³².

In the case of metallic powders, the value of stability index is around 1, which means that they are stable powders, and their shape and size do not change during the blade action in the test, as seen usually with ceramic powders³².

However, regarding FRI values, blended powder shows a slightly higher FRI ($\text{FRI} = 1.46 \pm 0.045$) than the AA 2017 powder ($\text{FRI} = 1.28 \pm 0.005$). Their greater interlocking and cohesion favor more air entrapping among particles. Indeed, during the test, there is a likelihood of air escape from powder layers, thus increasing the interlock among particles, making it more challenging to move the blade within the powder as the blade speed decreases, especially for the blended powder. This behavior demonstrates that blended powder may be more sensitive to the variation in the flow rate and needs special attention when handled within the L-PBF process because the flow rate may vary inside powder feeders as well as the speed of the powder spreading system.

3.3.2. Powder characterization under aerated condition

The amount of air present influences how the particles interact with each other, which directly affects the flow

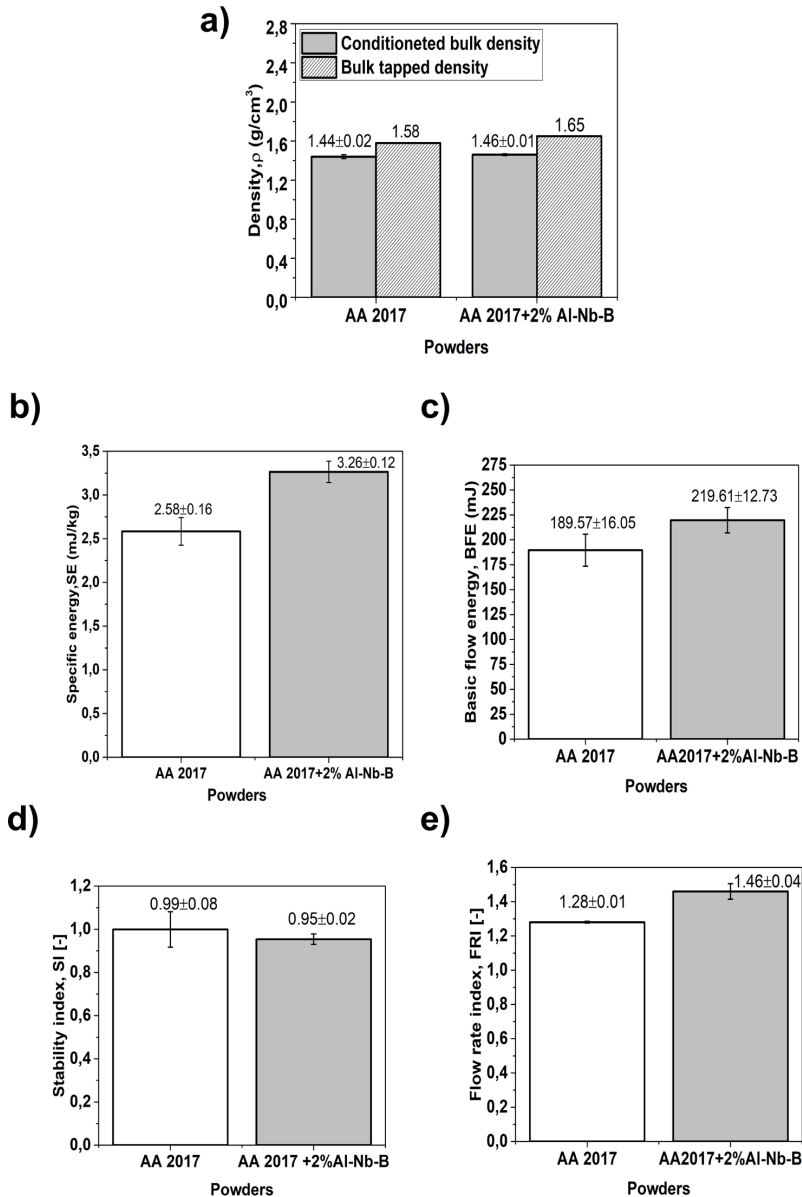


Figure 5. Parameters measured in free surface and packed condition: (a) conditioned bulk density (CBD) and tap bulk density (bulk density tap_{50}), (b) specific energy (SE), (c) basic flow energy (BFE), (d) stability index (SI), and (e) flow rate index (FRI).

properties³⁵. This phenomenon can be seen in the graph of Aerated Energy (AE) versus Air velocity (Figure 6a), where the powder bed is fully fluidized when AE is lower than 10 mJ or even better, tend to zero according to the rheometer manufacturer³⁵. In this work, with no air insertion, both powders show difficulty in flowing. However, the AA 2017 powder shows lower AE ($\text{AE} = 274 \pm 35.4 \text{ mJ}$) than the blended powder ($\text{AE} = 330 \pm 29.6 \text{ mJ}$) due the blended powder has more agglomerated particles, which may hinder slip among particles and, consequently decrease the flowability³⁹.

For the blended powder, the fluidization starts to happen at 2 mm/s and for the AA 2017 powder at 4 mm/s, as presented in Figure 6a. In other words, when nitrogen velocity reaches

2 mm/s, the energy needed to move blended powder is reduced by practically half compared to AA 2017 powder. However, this may mean blended powder is more sensitive to aeration since gas flow easily passes through the finest particles, which are also carried away easily flowed by gas movement due to their lower mass.

For higher air velocity values, the fluidization of both powders suggests they would behave comparably as long as gas flow is maintained. This may indicate that it might be interesting to apply a certain flow of gas during the formation of the powder bed. Directly extracted from the aeration test, the fluidization capability of the powders was also measured through Aeration Ratio (AR), as shown in Figure 6b, which means they

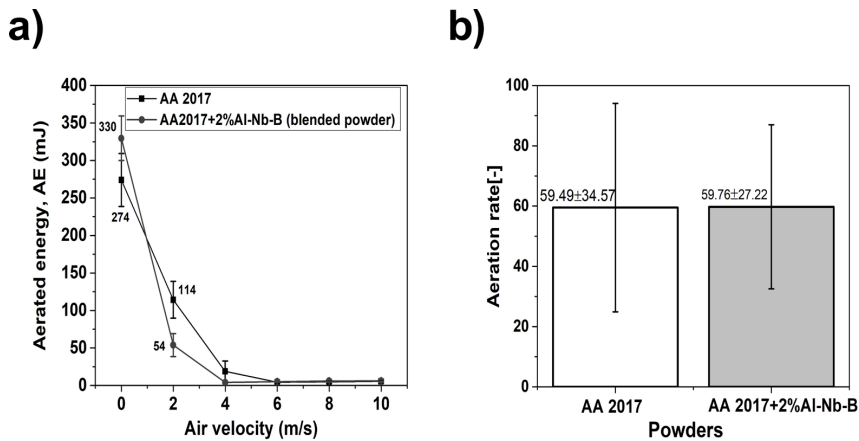


Figure 6. Parameters measured in aerated condition: (a) Aerated energy and (b) Aeration rate.

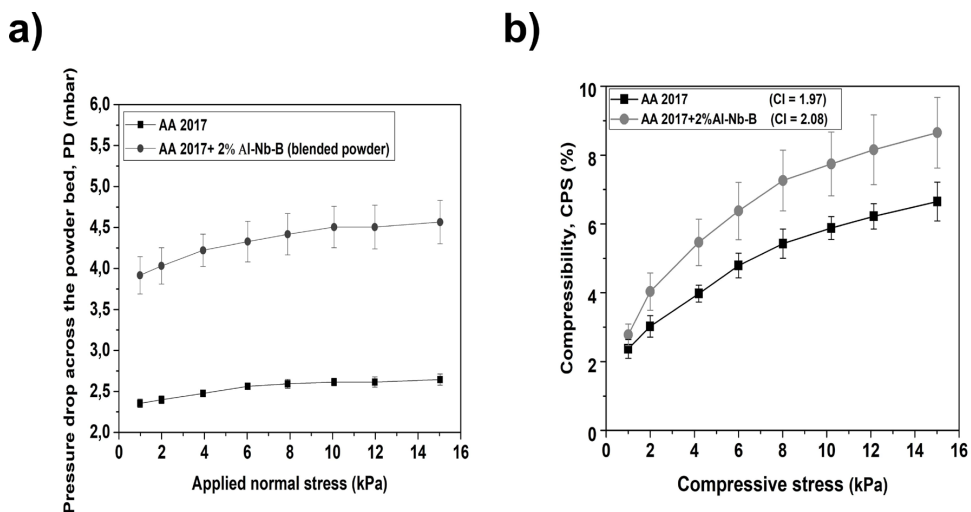


Figure 7. Parameters measured under packed condition: (a) pressure drop across the powder bed, and (b) compressibility.

are low-cohesion powders, according to the powder rheometer manufacturer³⁵.

3.3.3. Powder characterization under packed condition

The permeability variation as the pressure drops across the powder bed versus normal stress is illustrated in Figure 7a. The blended powder shows a significantly higher pressure drop than AA 2017 powder, which indicates it is less permeable. This means that air will have a tendency to be retained in the layer during the deposition and spreading process, which can result in poor layer uniformity, leading to imperfections in the final product^{48,50}. In addition, as the powder is compressed, the void fraction is reduced, and therefore the pressure drop is more remarkable for the blending powder due to its narrower distribution. The AA 2017 powder has a broader PSD, resulting in lower packing in the test tension condition and facilitating air passage.

This result is closely linked to the compressibility metric, as shown in Figure 7b, where powders exhibiting high compressibility tend to have high flow energy and,

consequently, an inefficient formed powder bed^{39,49}. It is worth mentioning that this is a measure of volume change in a powder sample due to an applied consolidating stress. This is not to be confused with the traditional compressibility test in the powder metallurgy based on external force, but how much force must be applied by the spreading system to ensure a homogeneous powder bed. In this respect, AA 2017 stands apart from both the lowest compressibility percentage and the consolidation index (CI=1.97) compared to blended powder (CI=2.08). Despite the increase in applied pressure, voids may have remained among the particles of AA 2017 powder, in contrast to the blended powder, which exhibits higher densification due to the presence of finer particles to fill the voids.

Considering findings, AA 2017 powder appears to be more suitable for obtaining a homogeneous and denser bed because of its better permeability. That is, it has a better ability to release the air trapped among the particles and require a lower pressure to rearrange the particles during powder bed formation, which is consistent with Brika et al.⁵¹.

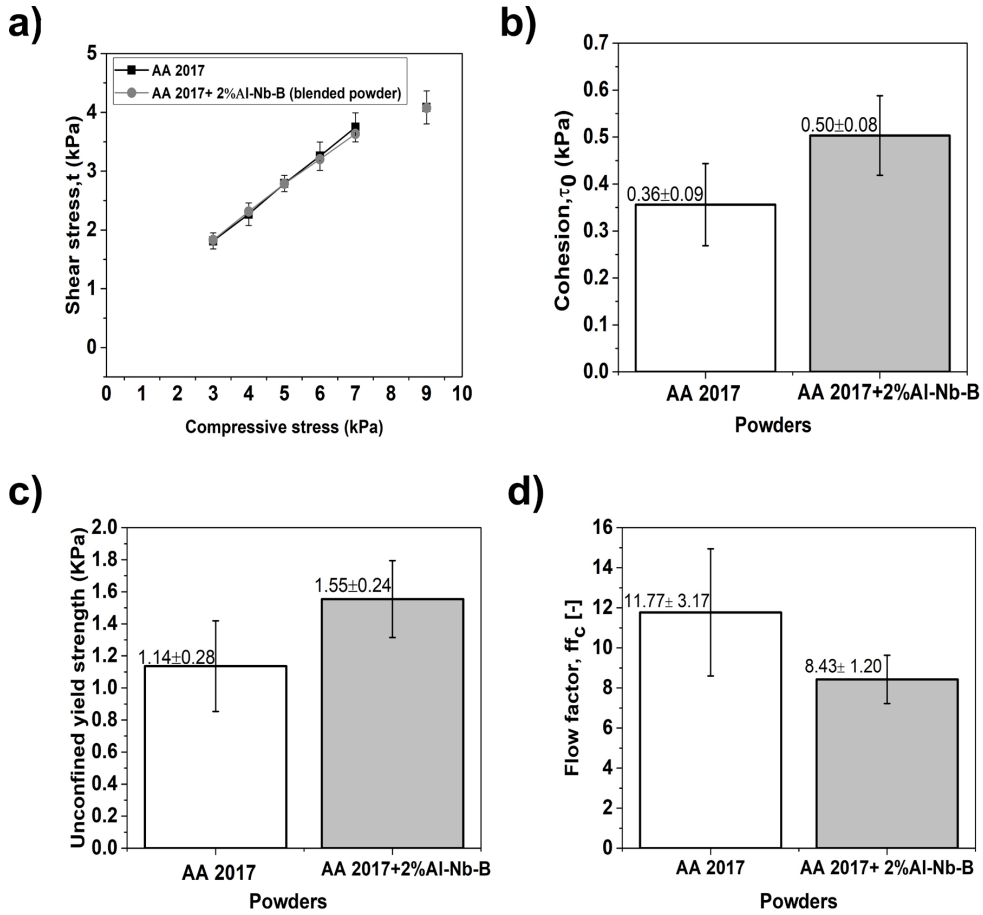


Figure 8. Parameters measured in shear condition: (a) shear stress, (b) cohesion, (c) unconfined yield strength and (d) flow factor.

3.3.4. Powder characterization under shear condition

The shear test can confirm the friction between particles, where the powder initially resists torsional movement, and then the shear stress increases until it reaches the yield stress, where the interaction between the particles is broken. From the stress curves obtained (as illustrated in Figure 1), the Mohr stress circle analysis resulted in three important values: cohesion (τ_0), Unconfined Yield Strength (σ_c), and Flow Fraction (ff_c), which are presented in Figure 8. In general, the shear stress was slightly equal for both powders (Figure 8a), but the AA 2017 powder showed the lowest cohesion strength, and unconfined yield stress (Figures 8b and 8c), while for flow factor (ff_c) was four times as high compared to the blended powder (Figure 8d). According to Langlais et al.³⁹, a low cohesion value indicates good flowability since this metric can be understood as nominal shear stress required to initiate flow when no normal strength is applied. However, a higher Flow Factor value denotes higher flowability when a highly consolidated powder shows a weak internal strength, in other words, low forces of interaction among particles.

From these results, it is possible to affirm that the blended powder tends to show greater difficulty in flowing within the process, leading to feeding funnel clogging and, consequently, stoppage of powder layer formation.

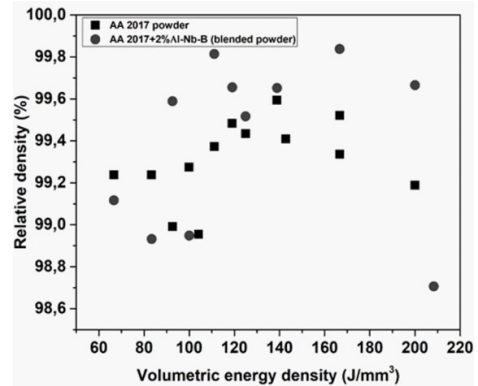


Figure 9. Relative density versus volumetric energy density for AA 2017 and blended powder (AA 2017+ 2% Al-Nb-B) samples produced by laser-based powder bed fusion.

3.4. L-PBF parameter optimization and densification

Figure 9 shows the relationship between relative density with the volumetric energy density of the samples produced using AA 2017 powder and the blended powder. Although the blended powder exhibits low flowability behavior, the majority of L-PBF

samples that used it are nearly fully dense, with a relative density ($\geq 99.6\%$) higher than that of the AA 2017 samples ($\sim 99.4\%$). Despite the scattered results, it is not possible to identify a relative density difference between cubes made with the two distinct powders. Further details on the inoculant's critical role in modifying the solidification behavior of the AA2017 during L-PBF processing will be discussed in future work.

4. Conclusion

Although the powder blending method has stood out as a cost-saving route for obtaining new aluminum alloys for the L-PBF process, the traditional characterization methods such as sieving and tools (Hall and Carney's funnel) did not differentiate between powders. Given the complexity of understanding and modeling flowability behaviors and many factors that affect flow properties such as particle size distribution, particle morphology, roughness, material density, and the electrostatic and interparticle forces, a more systematic study is necessary. This work investigated the physical characteristics and rheological properties of powders under four dry test conditions (dynamic, aerated, packed, and shear). The following conclusions were drawn:

- The addition of Al-5.0Nb-0.5B inoculant powder in AA2017 matrix powder impacted the final powder blending composition, morphology, and rheological performance in the L-PBF process.
- The finer particles of the inoculant powder resulted in a smaller span of the blended powder, which concentrated the particle size distribution around the 11 to 33 μm range. The increased presence of fine particles and agglomerates led to a decrease in the powder's flowability.
- The AA 2017 powder displayed more spherical morphology and slightly less agglomerated particles than the blended powder, which, in turn, directly impacted flowability behavior.
- The blended powder has higher SE and BFE than AA2017 powder, suggesting it is more cohesive in dynamic conditions, such as filling and spreading to form a powder bed. However, the first powder is more sensitive to nitrogen flow due to the absence of the inoculant particles.
- Regarding packed condition, blended powder showed a significantly high-pressure drop, indicating its ability to retain air in the powder layers. Thus more difficult it is to air may pass, the more likely it is to don't show a flow freely, which can result in poor powder bed uniformity. In addition, it showed a higher degree of compressibility, which indicates its high cohesivity; therefore, additional stress is required to overcome adhesion between the particles.
- AA 2017 powder clearly displayed the lowest degree of friction and cohesion among particles during the shear condition, evidencing its ease to inducing flow compared to blended powder.
- Although rheological indices indicated that the addition of the inoculant negatively affects powder flowability, it is was not possible to establish a correlation between these rheological indices and the properties of parts produced by the L-PBF process.

Finally, the insights into physical properties coupled with results obtained through systematic rheological tests can help assess the powder's flowability behavior after the blending process and are a rapid alternative to glimpse the flow behavior of powders during the L-PBF process.

5. Acknowledgments

The authors would like to thank the Brazilian research funding agencies – This study was financed in part by the Coordenação de Aperfeiçoamento de Pessoal de Nível Superior- Brasil (CAPES) - Finance code 001, São Paulo Research Foundation – FAPESP [Grant 2017/27031-4, Grant 2019/13715-4, Grant 2020/09544-7 and Grant 2022/05528-2] and National Council of Technological and Scientific Development – Brazil / CNPQ [Grant 167845/2018-7]. Additionally, the Laboratory of Structural Characterization of Department of Materials Engineering at the Federal University of São Carlos (LCE/DEMa/UFSCar) and Center Characterization and Development Materials (CCDM/DEMa/UFSCar) for the microscopy facilities, Laboratory of Metallurgical Processes, Institute for Technological Research (LPM/ IPT) for powder characterization infrastructure and CBMM Company donated Al-5.0Nb-0.5B inoculant ingots.

6 References

1. Tan Q, Zhang J, Sun Q, Fan Z, Li G, Yin Y, et al. Inoculation treatment of an additively manufactured 2024 aluminium alloy with titanium nanoparticles. *Acta Mater.* 2020;196:1-16.
2. Wang Z, Wang X, Chen X, Qiu C. Complete columnar-to-equiaxed transition and significant grain refinement in an aluminium alloy by adding Nb particles through laser powder bed fusion. *Addit Manuf.* 2022;51:102615.
3. Zhang D, Prasad A, Bermingham MJ, Todaro CJ, Benoit MJ, Patel MN, et al. Grain refinement of alloys in fusion-based additive manufacturing processes. *Metall Mater Trans, A Phys Metall Mater Sci.* 2020;51(9):4341-59.
4. Li G, Jadhav SD, Martín A, Montero-Sistiaga ML, Soete J, Sebastian MS, et al. Investigation of solidification and precipitation behavior of Si-modified 7075 aluminum alloy fabricated by laser-based powder bed fusion. *Metall Mater Trans, A Phys Metall Mater Sci.* 2021;52(1):194-210.
5. Agarwal G, Kumar A, Gao H, Amirthalingam M, Moon SC, Dippenaar RJ, et al. Study of solidification cracking in a transformation-induced plasticity-aided steel. *Metall Mater Trans, A Phys Metall Mater Sci.* 2018;49(4):1015-20.
6. Agarwal G, Kumar A, Richardson IM, Hermans MJM. Evaluation of solidification cracking susceptibility during laser welding in advanced high strength automotive steels. *Mater Des.* 2019;183:108104.
7. Zhang J, Gao J, Song B, Zhang L, Han C, Cai C, et al. A novel crack-free Ti-modified Al-Cu-Mg alloy designed for selective laser melting. *Addit Manuf.* 2021;38:101829.
8. Agrawal P, Gupta S, Thapliyal S, Shukla S, Haridas RS, Mishra RS. Additively manufactured novel Al-Cu-Sc-Zr alloy: microstructure and mechanical properties. *Addit Manuf.* 2021;37:101623.
9. Martín JH, Yahata B, Mayer J, Mone R, Stonkevitch E, Miller J, et al. Grain refinement mechanisms in additively manufactured nano-functionalized aluminum. *Acta Mater.* 2020;200:1022-37.
10. Xiao F. Preface. *J Alloys Compd.* 2022;404-406:1.
11. Araújo APM, Micheloti L, Kiminami CS, Bolfarini, C. Uhlenwinkel V, Gargarella P. Morphological and microstructural

- characterization of Al95Fe2Cr2Ti1 powders produced by two different gas atomizers. *Tecnol Metal Mater Min.* 2021;18:e2316.
12. Marchetti L, Hulme-Smith C. Flowability of steel and tool steel powders: a comparison between testing methods. *Powder Technol.* 2021;384:402-13.
 13. Muñoz-Lerma JA, Nommets-Nom A, Waters KE, Brochu M. A comprehensive approach to powder feedstock characterization for powder bed fusion additive manufacturing: a case study on AlSi7Mg. *Materials.* 2018;11(12):2386.
 14. Vock S, Klöden B, Kirchner A, Weißgärber T, Kieback B. Powders for powder bed fusion: a review. *Prog Addit Manuf.* 2019;4(4):383-97.
 15. Strondl A, Lyckfeldt O, Brodin H, Ackelid U. Characterization and control of powder properties for additive manufacturing. *J Miner Met Mater Soc.* 2015;67(3):549-54.
 16. Weaver JS, Whiting J, Tondare V, Beauchamp C, Peltz M, Tarr J, et al. The effects of particle size distribution on the rheological properties of the powder and the mechanical properties of additively manufactured 17-4 PH stainless steel. *Addit Manuf.* 2021;39:101851.
 17. Chen H, Chen Y, Liu Y, Wei Q, Shi Y, Yan W. Packing quality of powder layer during counter-rolling-type powder spreading process in additive manufacturing. *Int J Mach Tools Manuf.* 2020;153:103553.
 18. Cordova L, Bor T, de Smit M, Campos M, Tinga T. Measuring the spreadability of pre-treated and moisturized powders for laser powder bed fusion. *Addit Manuf.* 2020;32:101082.
 19. Huck-Jones D, Langley C. Beyond particle size: exploring the influence of particle shape on metal powder performance. *Metal Am.* 2017;3(4):99.
 20. Coe HG, Pasebani S. Use of bimodal particle size distribution in selective laser melting of 316L stainless steel. *J. Manuf Mater Process.* 2020;4(1):8.
 21. Besterci M, Käerdi H, Kulu P, Mikli V. Characterization of powder particle morphology. *Proc Est Acad Sci Eng.* 2001;7:22-34.
 22. Whiting JG, Tondare VN, Scott JHJ, Phan TQ, Donmez MA. Uncertainty of particle size measurements using dynamic image analysis. *CIRP Ann.* 2019;68(1):531-4.
 23. ASTM: American Society for Testing and Materials. ASTM F3049-14. standard guide for characterizing properties of metal powders used for additive manufacturing processes. West Conshohocken: ASTM; 2014.
 24. Sun YY, Gulizia S, Oh CH, Doblin C, Yang YF, Qian M. Manipulation and characterization of a novel titanium powder precursor for additive manufacturing applications. *J Miner Met Mater Soc.* 2015;67(3):564-72.
 25. Shah UV, Karde V, Ghoroi C, Heng JYY. Influence of particle properties on powder bulk behaviour and processability. *Int J Pharm.* 2017;518(1-2):138-54.
 26. Aboulkhair NT, Simonelli M, Parry L, Ashcroft I, Tuck C, Hague R. 3D printing of Aluminium alloys: additive manufacturing of aluminium alloys using selective laser melting. *Prog Mater Sci.* 2019;106:100578.
 27. Wang P, Gammer C, Brenne F, Niendorf T, Eckert J, Scudino S. A heat treatable TiB2/Al-3.5Cu-1.5Mg-1Si composite fabricated by selective laser melting: Microstructure, heat treatment and mechanical properties. *Compos, Part B Eng.* 2018;147:162-8.
 28. Elambasseril J, Benoit MJ, Zhu S, Easton MA, Lui E, Brice CA, et al. Effect of process parameters and grain refinement on hot tearing susceptibility of high strength aluminum alloy 2139 in laser powder bed fusion. *Prog Addit Manuf.* 2022;7(5):887-901.
 29. Micrometrics Instrument Corporation. Particle insight: particle shape analyzer Norcross, GA; 2008. 80 p.
 30. ASTM: American Society for Testing and Materials. ASTM B923-10: standard test method for metal powder skeletal density by helium or nitrogen. West Conshohocken: ASTM; 2015. 10 p.
 31. Freeman Technology. Density methods. Tewkesbury; 2006. (vol. 1).
 32. Freeman Technology. Specific energy method. Tewkesbury; 2008. (vol. 2).
 33. Freeman Technology. Basic flowability energy method. Tewkesbury; 2013. (vol. 8).
 34. Freeman Technology. Tapped consolidation method. Tewkesbury; 2013. (vol. 4).
 35. Freeman Technology. Aeration method. Tewkesbury; 2013. (vol. 9).
 36. Freeman Technology. Permeability method. Tewkesbury; 2009. (vol. 1).
 37. Freeman Technology. Compressibility method. Tewkesbury; 2013. (vol. 5).
 38. ASTM: American Society for Testing and Materials. ASTM D7891-15: standard test method for shear testing of powders using the Freeman Technology. West Conshohocken: ASTM; 2020.
 39. Langlais D, Demers V, Brailovski V. Rheology of dry powders and metal injection molding feedstocks formulated on their base. *Powder Technol.* 2022;396:13-26.
 40. Wang P, Gammer C, Brenne F, Prashanth KG, Mendes RG, Rummeli MH, et al. Microstructure and mechanical properties of a heat-treatable Al-3.5Cu-1.5Mg-1Si alloy produced by selective laser melting. *Mater Sci Eng A.* 2018;711:562-70.
 41. ASTM: American Society for Testing and Materials. ASTM B962-13: standard test methods for density of compacted or sintered Powder Metallurgy (PM) products using Archimedes' principle. West Conshohocken: ASTM; 2013.
 42. Baitimerov R, Lykov P, Zhrebtsov D, Radionova L, Shults A, Prashanth KG. Influence of powder characteristics on processability of AlSi12 alloy fabricated by selective laser melting. *Materials.* 2018;11(5):742.
 43. Cordova L, Campos M, Tinga T. Revealing the effects of powder reuse for selective laser melting by powder characterization. *J Miner Met Mater Soc.* 2019;71(3):1062-72.
 44. Özbilen S. Satellite formation mechanism in gas atomized powders. *Powder Metall.* 1999;42(1):70-8.
 45. Li Y, Jiang Y, Liu B, Luo Q, Hu B, Li Q. Understanding grain refining and anti Si-poisoning effect in Al-10Si/Al-5Nb-B system. *J Mater Sci Technol.* 2021;65:190-201.
 46. Olakanmi EO, Cochrane RF, Dalgarno KW. A review on selective laser sintering/melting (SLS/SLM) of aluminium alloy powders: Processing, microstructure, and properties. *Prog Mater Sci.* 2015;74:401-77.
 47. Clayton J, Millington-Smith D, Armstrong B. The application of powder rheology in additive manufacturing. *J Miner Met Mater Soc.* 2015;67(3):544-8.
 48. Gao MZ, Ludwig B, Palmer TA. Impact of atomization gas on characteristics of austenitic stainless steel powder feedstocks for additive manufacturing. *Powder Technol.* 2021;383:30-42.
 49. Nguyen QB, Nai MLS, Zhu Z, Sun CN, Wei J, Zhou W. Characteristics of inconel powders for powder-bed additive manufacturing. *Engineering.* 2017;3(5):695-700.
 50. Freeman R. Measuring the flow properties of consolidated, conditioned and aerated powders: a comparative study using a powder rheometer and a rotational shear cell. *Powder Technol.* 2007;174(1-2):25-33.
 51. Brika SE, Letenneur M, Dion CA, Brailovski V. Influence of particle morphology and size distribution on the powder flowability and laser powder bed fusion manufacturability of Ti-6Al-4V alloy. *Addit Manuf.* 2020;31:100929.